atmosphere

MDPI

*Article*

# Intra-Seasonal Variations and Frequency of Major Sudden Stratospheric Warmings for Northern Winter in Multi-System Seasonal Hindcast Data

**Masakazu Taguchi**

Department of Earth Science, Aichi University of Education, Kariya 448-8542, Japan; mtaguchi@auecc.aichi-edu.ac.jp; Tel.: +81-566-26-2378

**Abstract:** This study investigates intra-seasonal variations and frequency of major sudden stratospheric warmings (MSSWs) in Northern winter seasonal hindcasts of six systems from 1993/1994 to 2016/2017, in comparison to the Japanese 55-year Reanalysis data. Results show that, over all, all systems reproduce precursory signals to the MSSWs well, such as the increase in the planetary wave heat flux in the extratropical lower stratosphere and the anomalous planetary wave patterns in the troposphere. Some systems are suggested to underestimate or overestimate the mean MSSW frequency. Such differences in the frequency of the MSSWs among the systems are related to those in the mean strength of the stratospheric polar vortex, and also may be partly contributed by those in the frequency of notable heat flux events. The hindcast data exhibit a weaker mean vortex and an increased MSSW frequency for a warm phase than for a cold phase of El Niño/Southern Oscillation, and for an easterly phase than for a westerly phase of the Quasi-Biennial Oscillation. These are qualitatively consistent with reanalysis results, except for a lower MSSW frequency for the warm phase in the reanalysis data. The reanalysis teleconnection results are larger in magnitude than the hindcast results for most ensemble members, although they are included near the edge of the distributions of the ensemble members. The changes in the MSSW frequency with the two external factors are correlated to those in the mean vortex strength among the ensemble members and also the ensemble means for some systems.

**Keywords:** sudden stratospheric warmings; intra-seasonal variations and frequency; Northern winter seasonal hindcasts



**Citation:** Taguchi, M. Intra-Seasonal Variations and Frequency of Major Sudden Stratospheric Warmings for Northern Winter in Multi-System Seasonal Hindcast Data. *Atmosphere* **2022**, *13*, 831. https://doi.org/10.3390/atmos13050831

Academic Editor: Jane Liu

Received: 26 April 2022
Accepted: 15 May 2022
Published: 19 May 2022



## 1. Introduction

Sudden stratospheric warmings (SSWs) are a spectacular phenomenon in the atmosphere during cold seasons, especially in the winter Northern Hemisphere (NH), in which the polar stratosphere warms largely and rapidly, accompanying strong deceleration or even a reversal of the polar night jet [1]. During SSWs, the stratospheric polar vortex, which normally encircles the polar region forming the polar night jet near its edge, exhibits large distortions, and sometimes even breaks down completely. SSWs typically accompany two-way dynamical coupling, i.e., typical intra-seasonal variability, between the stratosphere and troposphere. Upward coupling is contributed by planetary waves that originate and intensify in the troposphere, and propagate to the stratosphere [2–4]. Downward coupling is characterized by downward propagation of circulation anomalies from the stratosphere to the troposphere and surface initiated by the upward coupling [5–7]. Several processes have been proposed for the downward coupling, including the remote effect of stratospheric wave driving, and feedbacks of synoptic-scale and planetary-scale eddies in the troposphere [7–13]. The mean frequency of major SSWs (MSSWs) for NH winter, i.e., DJF (December, January, February), which are often defined as a reversal of the zonal mean zonal wind in the extratropical stratosphere at 60° N, 10 hPa, is about every two years [14,15].

Extratropical stratospheric variability, especially the occurrence of MSSWs, can increase sub-seasonal and seasonal predictability of tropospheric and surface weather conditions. A study demonstrated that seasonal forecasts initialized on the onset date of observed MSSWs had enhanced skill for surface weather conditions for a time range of 16–60 days, compared to unconditional forecasts [16]. Similar skill enhancement in sub-seasonal forecasts for surface circulation was shown, not only when the stratospheric polar vortex was anomalously weak, but also when it was extremely strong [17]. Domeisen et al. [18] showed that, for the Max Planck Institute Earth System Model, seasonal predictability of 500 hPa geopotential height (GPH) over Europe at lead times up to four months was increased only for El Niño winters that exhibited MSSWs. Scaife et al. [19] showed that the Met Office Global Seasonal forecast system had high correlation skill in forecasting the winter North Atlantic Oscillation, but the skill essentially disappeared when ensemble members containing MSSWs were excluded. Mukougawa et al. [20] claimed that the prediction skill for the upper tropospheric Northern Annular Mode (NAM) improved for a 5–13 day forecast when initial states included negatively large NAM around 30 hPa in comparison to a positive NAM counterpart.

It is, therefore, essential to understand extratropical stratospheric variability in sub-seasonal and seasonal forecasts, so as to fully utilize its role in tropospheric and surface weather predictability. Sub-seasonal forecasts, in addition to climate simulations, have been extensively studied in terms of extratropical stratospheric variability, such as MSSWs [21–27], whereas seasonal forecasts remain relatively unexplored.

Regarding climatological features in seasonal forecasts, Maycock et al. [28] examined simulations of the NH winter extratropical stratospheric circulation in five seasonal forecast models from the ENSEMBLES project, with a top ranging from about 5 to 10 hPa. Maycock et al. found that all models had a polar night jet that was too weak and located too equatorward, and that the models underestimated the number, magnitude, and duration of anomalous states. Furtado et al. [29] examined NH winter seasonal hindcasts of three North American Multi-Model Ensemble Phase-2 models in terms of intra-seasonal variations of MSSWs. The examination identified model biases, such as an underestimation of intra-seasonal stratospheric variability, inconsistent precursory GPH fields, and weaker-than-observed wave activity prior to the MSSWs. Two of the three models, in addition to the Max Planck Institute Earth System Model, had a realistic MSSW frequency, whereas the remaining one has a much lower frequency [18,29]. Portal et al. [30] examined five seasonal forecast systems in the Copernicus Climate Change Service (C3S) multi-model database, and found that four of the five systems had a realistic MSSW frequency, with one exceptional system exhibiting a reduced frequency. Previous studies pointed out that differences in the MSSW frequency among different climate models were related to those in the mean vortex strength [24,31–33].

As for teleconnection signals in seasonal forecasts, the Max Planck Institute Earth System Model well reproduced the El Niño teleconnection to the extratropical stratosphere, including a deepened Aleutian low and an enhanced planetary wave of zonal wave number one (wave 1) connected to a weak and warm anomaly of the polar vortex [18] (see also Domeisen et al. [34] for a review of the teleconnection of El Niño/Southern Oscillation (ENSO)). Using the Climate-system Historical Forecast Project data, Butler et al. [35] found that high-top models tended to have a more realistic response of the extratropical stratosphere to El Niño and QBO (i.e., warmer and weaker polar vortex for El Niño and QBO easterly phase) compared to low-top models (see Anstey and Shepherd [36] and Anstey et al. [22] for reviews of the QBO teleconnection). Several mechanisms linking the QBO to vortex variability, such as MSSWs, have been proposed, including effects of the changes in the zonal mean zonal wind and meridional circulation [37–40], and radiative effects of ozone waves [41]. Portal et al. [30] found that the C3S systems overestimated the stratospheric response to ENSO and underestimated the influence of the QBO. Fereday et al. [42] found in seasonal hindcast data that the MSSW frequency was enhanced when NINO3.4 index was higher and the QBO was in the easterly phase.

This study investigates extratropical stratospheric variability, in particular MSSWs, in seasonal hindcast data for NH winter from both climatological and also teleconnection perspectives, in comparison to data for the real world, i.e., the Japanese 55-year Reanalysis (JRA-55) data. To be specific, we explore intra-seasonal variations of MSSWs, especially precursory signals, through a composite analysis. We also examine the frequency of MSSWs and relate this to the mean vortex strength and frequency of notable heat flux events. For the teleconnection perspective, we take account of ENSO and QBO as external factors since they are considered to be the most important factors to the NH extratropical stratosphere [43]. The HC data are taken from the C3S dataset, which was analyzed in Portal et al. [30], and the present analysis seeks to further improve understanding extratropical stratospheric variability in seasonal forecast systems.

The rest of the paper is organized as follows. Section 2 documents data and analyses employed in this study. Section 3 describes analysis results from both climatological and teleconnection perspectives. Sections 4 and 5 provide discussion and conclusion, respectively.

## 2. Data and Analyses

### *2.1. Data*

This study examines seasonal HC data in comparison to observational and reanalysis data. Daily means of the JRA-55 reanalysis data [44] are used for atmospheric states in the real world. The use of the JRA-55 data is justified, since reanalysis data, including the JRA-55 data, are shown to have an overall good agreement in representing main features of MSSWs [45]. Examining other reanalysis data in the present context is beyond this study, and is left for future work. The monthly NOAA/CPC NINO3.4 index is used to classify ENSO conditions. The period of these data is from 1993/1994 to 2016/17 NH winter season, which is matched to that of the HC data.

For the HC data, this study targets seasonal HC for six systems initialized around early November from 1993 to 2016, and made available through the C3S database. The six systems chosen were available and provided daily data at 10 hPa in the database when the data were downloaded. Table 1 provides several features of the forecast systems. All base HC data for this study are daily data at 00Z. This study uses a later version for some systems and also adds JMA2, compared to Portal et al. [30]. It is also noted that all six systems can be regarded as high-top models if high-top models are defined as models having a top level at or above 1 hPa [26]. On the other hand, all five systems in [28] were low-top models. The system of the three in [29] that had a lower MSSW frequency was a low-top model.

**Table 1.** Summary of the six forecast systems analyzed in this study.

| System Name and Version Number, in Addition to Version Identifier | Resolution for Atmospheric Model [1] | Initial Date(s) | Ensemble Size | Threshold Correlation Values at 90 and 95% Levels [2] |
|---|---|---|---|---|
| ECMWF5<br>SEAS5 | $T_{CO}319$<br>L91<br>0.01 hPa | NOV01 | 25 | ±0.34, ±0.40 |
| UKMO15<br>GloSea5-GC2-LI | N216<br>L85<br>85 km | OCT09, 17, 25<br>NOV01 | 28 = 7 for each initial date | ±0.32, ±0.37 |
| METEOFRANCE7<br>System 7 | TL359<br>L91<br>1 hPa | Penultimate Thursday of OCT<br>Last Thursday of OCT<br>NOV01 | 25 = 12 (Penultimate Thu)<br>+12 (Last Thu)<br>+1 (NOV01) | ±0.34, ±0.40 |

**Table 1.** *Cont.*

| System Name and Version Number, in Addition to Version Identifier | Resolution for Atmospheric Model [1] | Initial Date(s) | Ensemble Size | Threshold Correlation Values at 90 and 95% Levels [2] |
|---|---|---|---|---|
| DWD21<br>GCFS2.1 | T127<br>L95<br>0.01 hPa | NOV01 | 30 | ±0.31, ±0.36 |
| CMCC35<br>SPS3.5 | 1/2° lat-lon<br>L46<br>0.2 hPa | NOV01 | 40 | ±0.26, ±0.31 |
| JMA2<br>CPS2 | TL159<br>L60<br>0.1 hPa | OCT13, 28 | 10 = 5 for each initial date | ±0.55, ±0.63 |

[1] Horizontal resolution, vertical levels, and top level. [2] A correlation coefficient value from N samples (N: ensemble size) is judged to be statistically significant at the confidence level of 90 or 95% (two side test) if it exceeds the designated threshold values. The threshold correlation values are ±0.73 and ±0.81 for the ensemble means of the six systems at the 90 and 95% levels, respectively. The threshold values are obtained using Student's t distribution.

We analyze the following quantiles:

- Zonal mean zonal wind at 60° N, 10 hPa. This measures the strength and flow direction of the stratospheric polar vortex. The long-term mean, i.e., over the 24 seasons, of the DJF mean zonal wind is used as the mean vortex strength (VS). The daily zonal wind data are also used to identify MSSWs.
- Poleward heat flux of waves 1–3 averaged over 45–75° N, 100 hPa. This represents planetary wave activity entering the extratropical stratosphere, since it is proportional to the vertical component of the Eliassen-Palm flux for the quasi-geostrophic scaling [4].
- GPH at 10 and 500 hPa. These are used for large-scale horizontal circulation patterns for the stratosphere and troposphere, respectively.
- The NINO3.4 index is used in the DJF means for an index of ENSO conditions. The HC SST data are spatially averaged over the NINO3.4 region (5° S–5° N, 170–120° W).
- Zonal mean zonal wind at Equator, 50 hPa is also used in the DJF means for an index of QBO conditions.

### 2.2. Analyses

We obtain anomalies of an arbitrary quantity in the daily HC data as follows. A climatology is first obtained as an average over all years and ensemble members for each system. The average is further smoothed with 31-day running mean to filter out fluctuations arising from the relatively small number of years. Then, for each ensemble member of each system, the anomalies for each date are extracted as deviations from the climatology. These procedures are applied to each spatial grid point. Anomalies of DJF mean data for the HC data are deviations from the long term and ensemble mean. The same procedures are also applied to the JRA-55 data, except that the JRA-55 data are just one realization.

We focus on the occurrence and frequency of MSSWs during winter, i.e., DJF period. An MSSW is identified as when the zonal mean zonal wind at 60° N, 10 hPa is reversed from a westerly wind to an easterly wind for DJF. This is a common identification procedure discussed in [14,15,46]. In order to avoid a double count of one event, a condition that the zonal wind must be westerly for 20 days before a wind reversal date is required for the reversal to be identified as an MSSW. The date of the wind reversal is referred to as the MSSW central date and denoted as lag = 0 day.

We also identify notable heat flux events (HFEs) using the waves 1–3 heat flux data. To this end, we first obtain time mean heat flux anomalies for each date t, which are taken

for $\tau + 1$ days from $t - \tau$ to t. We then identify an HFE event if the time mean anomalies exceed a specified threshold. The date of the exceedance is referred to as the HFE central date and lag = 0 day. The anomalies must not exceed the threshold for 2*tau days before the central date. The time mean seeks to avoid using relatively noisy daily heat flux data, and uses $\tau$ = 10 days and threshold of 14 K m/s based on a composite analysis with respect to MSSWs.

The DJF mean NINO3.4 index for the real world and each ensemble member of each system is used to classify each DJF season into either of the three ENSO conditions: LA for La Niña, NT for neutral, and EL for El Niño condition. The LA and EL winters are when the NINO3.4 index exceeds $\pm$0.75 standard deviation (inclusive). The other winters are classified as NT. Similarly, the DJF mean QBO index is used to classify each DJF season into either of the two QBO conditions: ELY for easterly, and WLY for westerly condition. The WLY winters are when the QBO index is equal to, or larger than, 0 m/s, and the other winters are classified as ELY. We compare results for six conditions in Section 3.2, which includes ALL for all winters as a reference in addition to the above five conditions.

The following analyses use the correlation coefficient to examine possible relationships between target quantities. A correlation coefficient value is judged to be statistically significant if it exceeds a threshold value determined by Student's t distribution. The threshold value depends on the sample size and confidence level. Table 1 lists the threshold values for the 90 and 95% levels (two side test) when examining the ensemble members for each system. Student's *t* test is also used to examine if an ensemble mean value calculated from the ensemble members is significantly different from zero (two side test).

## 3. Results

### *3.1. Climatological Features*

Figure 1a,b overview climatological features of the stratospheric polar vortex in the mean VS and MSSW frequency. The panels plot the 99% range (0.5 to 99.5 percentile) of each quantity using all ensemble members for each system, in addition to the ensemble mean. The climatological VS of the six systems is distributed around the JRA-55 data. It is weaker for the four systems than for the JRA-55 data, and stronger for the other two systems (Figure 1a). The mean MSSW frequency is also distributed around the JRA-55 data (Figure 1b). The 99% range of ECMWF5 is higher than the JRA-55 result. The JRA-55 result is near the lower end of the range for UKMO15, METEOFRANCE7, and DWD21. This implies that most of the ensemble members of these systems have a higher MSSW frequency than the JRA-55 counterpart. The situation is opposite for JMA2. The following examines intra-seasonal variations of the extratropical stratosphere and troposphere around the MSSWs, and then the frequency of the MSSWs.

A composite analysis with respect to the MSSW central date is conducted to examine intra-seasonal variations around the MSSWs (Figure 2). All systems and JRA-55 data commonly show strong wind decelerations and heat flux increases in an about 10-day period before the central date when the zonal wind becomes negative. Such a close connection between stratospheric polar vortex and lower stratospheric wave activity variations in the HC data was shown by [30]. Composite zonal wind anomalies exhibit stronger (more negative) anomalies for CMCC35 and JMA2. This reflects that the criterion of the zonal wind reversal for MSSWs requires stronger decelerations for systems of a stronger westerly wind. Composite heat flux anomalies also stand out for CMCC35. Such heat flux increases prior to MSSWs can be understood from the viewpoint of interference between climatological and anomalous fields [47–50].

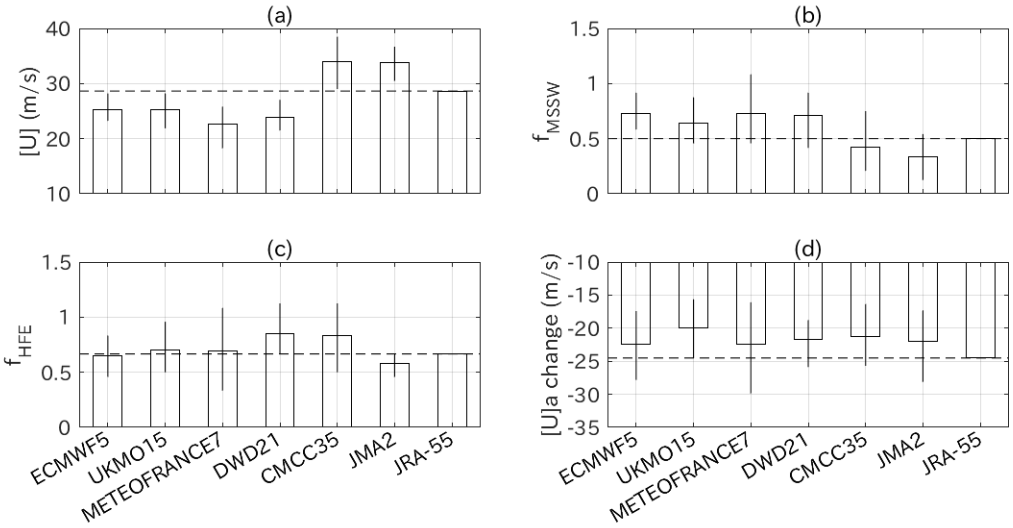


**Figure 1.** Bar charts of four quantities relevant for the stratospheric polar vortex for the HC and JRA-55 data: (**a**) climatological zonal mean zonal wind [U] at 60° N, 10 hPa, (**b**) frequency of MSSWs, (**c**) frequency of HFEs, and (**d**) mean time change in zonal wind anomalies [U]a from lag = −10 to 0 day for the HFEs. Panel (**a**) takes DJF means of the zonal wind, whereas (**b**,**c**) deal with events during DJF and plot their frequencies per DJF season. Each bar plots the ensemble mean, and each vertical line plots the 99% range of the ensemble members. Horizontal broken lines plot the JRA-55 results. Square brackets denote the zonal mean, and subscript a denotes anomalies.

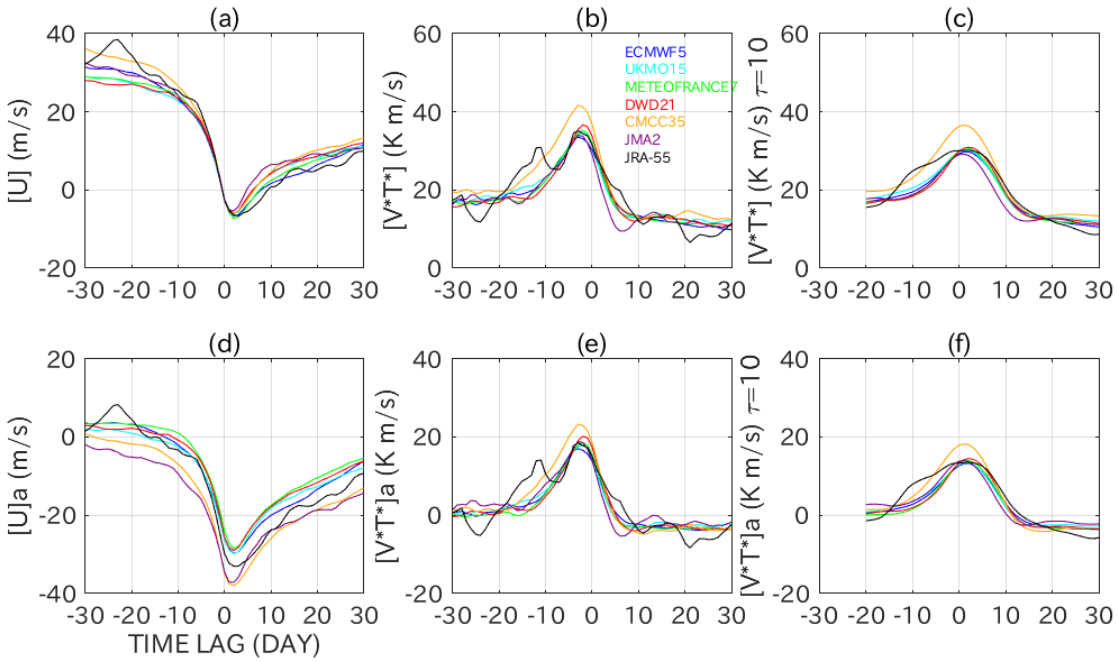


**Figure 2.** Ensemble means of composite time series with respect to the MSSW central date (lag = 0 day) for the HC and JRA-55 data: (**a**) zonal mean zonal wind at 60° N, 10 hPa, and (**b**) poleward heat flux of waves 1–3 in 45–75° N, 100 hPa, and (**c**) time mean of the heat flux. The time mean of the heat flux for each day is taken for 11 days from 10 days before the day to it (i.e., $\tau$ = 10 days). The composites are taken for the MSSWs in each ensemble member, and the results are averaged across the members. Panels (**d**–**f**) are for anomalies of the three quantities. Color legend is shown in (**b**). Asterisk denotes wave components, i.e., deviations from the zonal mean.

Separate contributions from wave 1 and wave 2 to the increased heat flux are further examined in Figure 3. The figure plots the ensemble mean result (dot) and representative

distribution of the ensemble members (ellipse) for each system. The ellipse is extracted by applying empirical orthogonal function (EOF) analysis to the results of the ensemble members. The climatological wave 1 and wave 2 heat fluxes are distributed near the JRA-55 data for the five systems, except for CMCC35, which is biased toward a stronger wave 1 contribution (Figure 3a). Even for the five systems, the JRA-55 result is located near the edge of each ellipse. For example, a large part of the ensemble members of METEOFRANCE7 have a weaker wave 1 contribution and a stronger wave 2 contribution. JMA2 is suggested to have a smaller sum of the two components, i.e., weaker planetary wave activity. It is interesting to note that the ensemble members for each system exhibit a negative correlation ranging from −0.66 to −0.47, i.e., compensation between the two components. Some of these biases are reflected in the composite results, e.g., for CMCC35 and METEOFRANCE7, although the variability among the ensemble members is large and the ellipse of each system covers the JRA-55 result (Figure 3b). The differences among the systems become inconspicuous in the composite anomalies (Figure 3c).

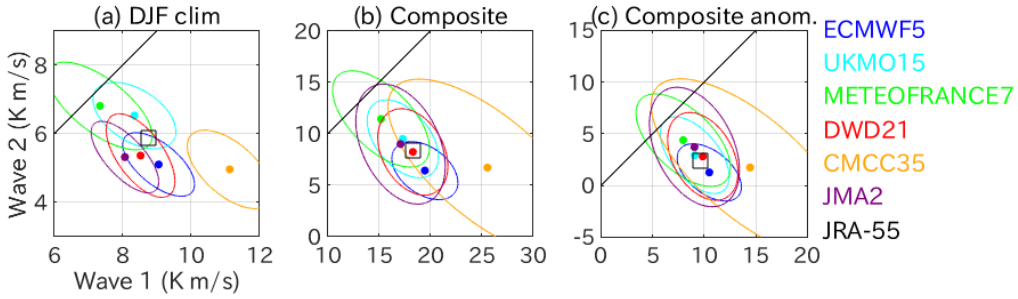


**Figure 3.** (**a**) Scatter plot between the climatological wave 1 and wave 2 heat flux (*x* and *y* axis, respectively) in 45–75° N, 100 hPa during DJF. Each dot plots the ensemble mean result for each system. Each ellipse plots a representative distribution of the ensemble members for each system. The directions of the long and short axes are extracted by EOF analysis. The length of each axis is the 99 percentile of the distance values, from the center of the ellipse to the ensemble members projected onto the axis. Black square plots the JRA-55 result. Black line denotes the y = x line. Panel (**b**) is similar, but for the composite heat flux with respect to the MSSW central date. Time means are taken from lag = −10 to 0 day for both components. Panel (**c**) is similar to (**b**), but uses heat flux anomalies.

Since it is conceivable that the heat flux increases are associated with large scale tropospheric circulation anomalies, Figure 4 plots composite anomalies of the 500 hPa GPH averaged from lag = −10 to 0 day of the MSSWs in addition to the climatological state. The time window corresponds to the typical time scale of the heat flux increase at 100 hPa (Figure 2b,e). All six systems show similar patterns characterized by positive anomalies extending from north Canada to Europe, and negative anomalies over northeast Asia. These anomalies are roughly in phase with climatological wave 1, and hence act to strengthen wave 1 through constructive interference. This is consistent with the large contribution from wave 1 to the increased heat flux (Figure 3). The negative anomalies over northeast Asia are also seen in the JRA-55 data, although they seem more limited in zonal scale. The positive anomalies over north Atlantic and Europe are less conspicuous for the JRA-55 than for the HC data, whereas positive anomalies over North America are notable. These differences are likely to reflect the small sample size of the MSSWs in the JRA-55 data. These model and observational results are generally similar to previous studies [51,52].

A similar examination for the 10 hPa GPH around the MSSW onset date, i.e., from lag = −2 to +2 days, shows prevailing positive anomalies over the polar region for all systems and JRA-55 data, implying a weakening of the polar vortex (Figure 5). The positive anomalies have larger magnitudes for CMCC35 and JMA2, consistent with Figure 2d, as the climatological polar vortex is stronger for the two systems than for the other systems and JRA-55 data.

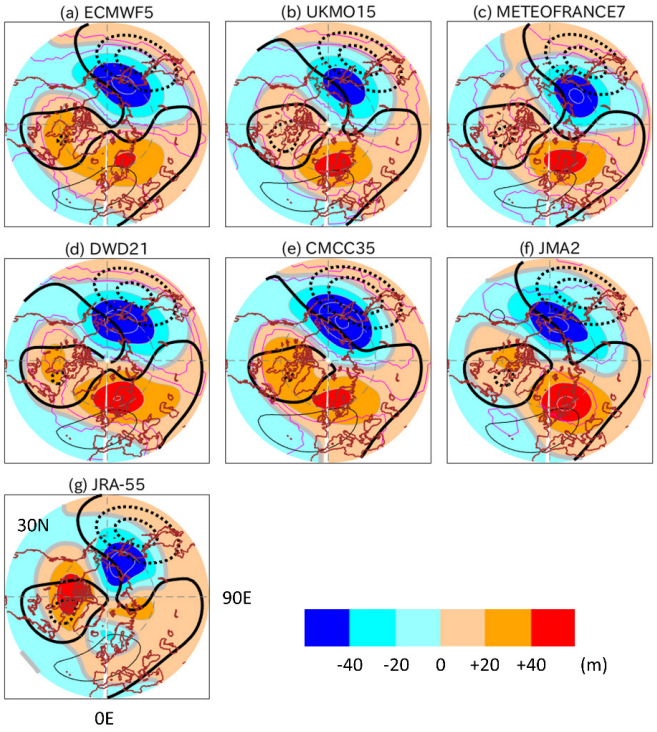


**Figure 4.** Ensemble mean composite maps of 500 hPa GPH anomalies for the HC and JRA-55 data, averaged from lag = −10 to 0 day of the MSSW central date (color shades) (**a**–**g**). Contour interval is 20 m. Only waves 1–3 components are retained. Magenta contours in (**a**–**f**) denote statistically significant anomalies at the 95% confidence level. Black contours show the waves 1–3 field in the DJF climatology in each data. Contour interval is 100 m. Solid black contours are for positive values (thick for zero), and dotted contours are for negative values.

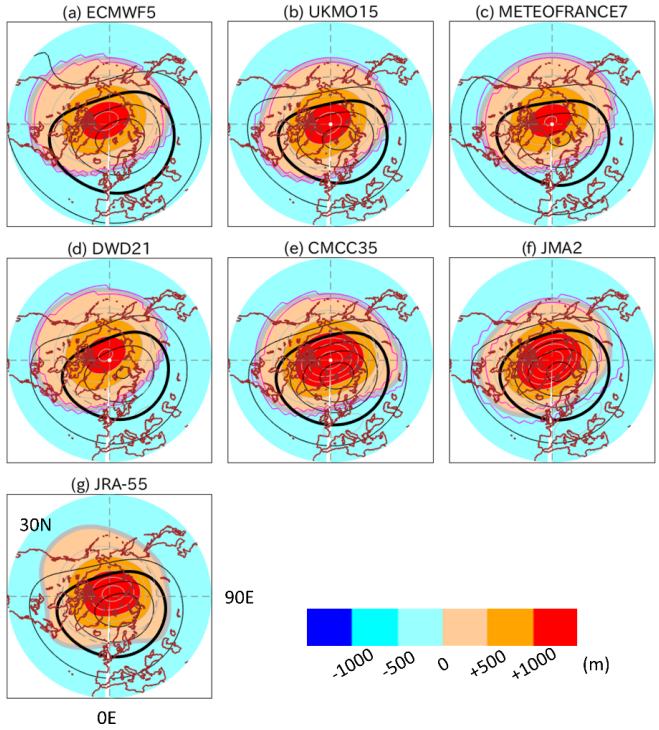


**Figure 5.** This is the same as Figure 4, but using the 10 hPa GPH from lag = −2 to +2 days. (**a**–**g**) All wave number components in addition to the zonal mean are retained. Contour interval is 250 m for the anomalies, and 500 m for the climatology. Thick black contour denotes 30,000 m.

Figure 1a,b suggested that the MSSW frequency is related to the mean VS, as pointed out by previous studies [24,31–33]. Such a relationship is examined for the present HC data in Figure 6a. The scatter plot shows their strong, linear relationship supporting the suggestion: the MSSW frequency is higher when the mean VS is weaker, and vice versa. The degree of the linear relationship is quantified using the correlation coefficient in Table 2. The table reveals strongly negative correlations for the ensemble members for each system and for the ensemble means of the six systems.

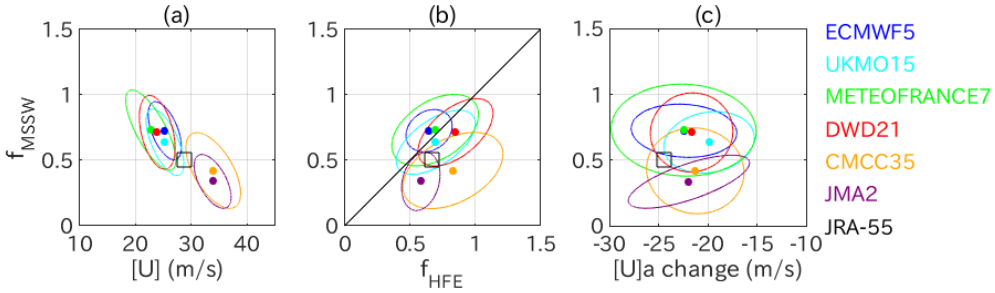


**Figure 6.** (**a**) Scatter plot between the climatological zonal mean zonal wind at 60° N, 10 hPa, and MSSW frequency, as plotted in Figure 3. Panel (**b**) uses the HFE frequency instead of the climatological zonal wind. Black diagonal line denotes the y = x line. Panel (**c**) uses the mean time change in anomalous zonal wind at 60° N, 10 hPa in response to the HFEs, i.e., from lag = −10 to 0 day.

**Table 2.** Correlation coefficient values between the key quantities. Three left columns correlate the MSSW frequency with the mean VS, HFE frequency, and mean time change in the anomalous zonal wind in response to the HFEs (see also Figure 6). The rightmost column correlates the mean VS with the HFE frequency. The values for each system are those among all ensemble members. The row "Ensemble means" uses the ensemble means from the six systems. Asterisk denotes statistical significance at the 95% level (see Table 1).

| System Name | $f_{MSSW}$ and Mean VS | $f_{MSSW}$ and $f_{HFE}$ | $f_{MSSW}$ and Mean [U]a Change | Mean VS and $f_{HFE}$ |
|---|---|---|---|---|
| ECMWF5 | −0.57 * | +0.20 | −0.094 | +0.18 |
| UKMO15 | −0.62 * | +0.39 * | +0.16 | −0.23 |
| METEOFRANCE7 | −0.66 * | +0.42 * | −0.031 | −0.12 |
| DWD21 | −0.46 * | +0.55 * | +0.028 | −0.22 |
| CMCC35 | −0.68 * | +0.40 * | −0.058 | −0.35 * |
| JMA2 | −0.64 * | +0.28 | +0.64 * | −0.14 |
| Ensemble means | −0.97 * | +0.19 | +0.040 | −0.11 |

The differences in the MSSW frequency among the ensemble members and systems may also be contributed to by those in transient variability [33], which is not directly included in the mean VS. This possibility is examined in terms of the frequency of notable HFEs in the lower stratosphere and the mean polar vortex response to them. The HFEs are identified as those comparable to the composite picture with respect to the MSSW central date (Figure 2, Section 2.2). Specifically, a time mean of the composite heat flux for each time lag is calculated for $\tau$ + 1 days from lag-$\tau$ to lag. A value of $\tau$ = 10 days is used as a representative time scale for the increase in the heat flux anomalies to the MSSWs (Figure 2c,e). The time mean composite heat flux anomalies for the MSSWs reveal a representative value of 14 K m/s around the MSSW onset date, and this value is used to identify the HFEs.

The ensemble mean HFE frequency of the six systems is again found to be distributed around the JRA-55 result (Figure 1c). The 99% range of DWD21 is above the JRA-55 result,

whereas that of JMA2 is below it. Possible correlations of the frequency of HFEs to that of the MSSWs are examined in Figure 6b and Table 2. The results reveal positive correlations, although they are statistically significant for the four systems. For such systems, except for CMCC35, the HFE frequency has an insignificant correlation with the mean VS (Table 2), so that it can be regarded as an additional factor to explain the MSSW frequency among the ensemble members. A similar relationship is also suggested for the ensemble means, although the correlation between the MSSW and HFE frequencies is insignificant. CMCC35 seems an outlier and acts to decrease the correlation.

It is also possible that the stratospheric polar vortex responds to the HFEs differently among the ensemble members and systems, and these differences contribute to the differences in MSSW frequency. Therefore, the HFEs are further used to conduct a composite analysis. A representative weakening response of the polar vortex to the HFEs is extracted as a mean time change of anomalous zonal wind at 60° N, 10 hPa from lag = −10 to 0 day, where the lag = 0 day refers to the central date of the HFEs (Figure 1d). The negative values in the figure mean that the anomalous wind decelerates in the 10-day time window. The ensemble means of all systems are weaker than the JRA-55 result, although the 99% range includes it. It is found that the vortex weakening response is not significantly correlated with the MSSW frequency for the ensemble members, except for JMA2, nor for the ensemble means (Figure 6c and Table 2). This metric is therefore excluded from the following analysis.

### *3.2. Teleconnection*

We next extend the above analysis in Section 3.1 to teleconnection signals with ENSO and QBO. Figure 7a,b overview the mean VS and MSSW frequency for the six conditions for the HC and JRA-55 data. One sees that for the ENSO teleconnection in the HC data the mean VS tends to weaken and the MSSW frequency tends to increase as the NINO3.4 index increases. Regarding the QBO teleconnection, the mean VS is weaker and the MSSW frequency is higher for ELY than for WLY, albeit weaker than for the JRA-55 data. Similar to Section 3.1, the following examines intra-seasonal variations around the MSSWs and the frequency of the MSSWs from a teleconnection perspective.

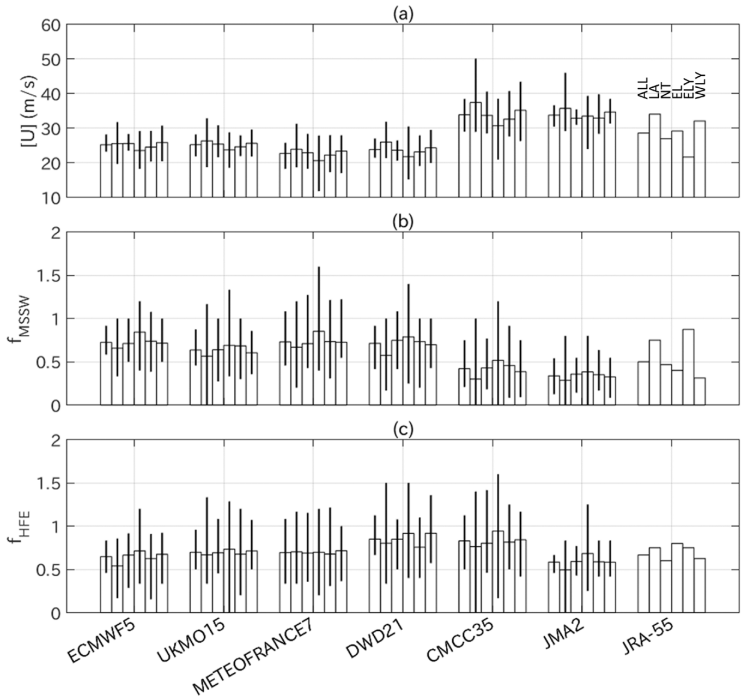


**Figure 7.** Similar to Figure 1a–c, but showing results for the six groups of ALL, LA, NT, EL, ELY, and WLY, which are explained in Section 2.2: (**a**) mean VS, (**b**) MSSW frequency, and (**c**) HFE frequency.

The composite analysis with respect to the MSSW central date is repeated using the MSSWs for each of the four conditions (Figure 8). The four conditions contrast the two opposite phases of ENSO (LA vs. EL, blue lines), and the two QBO phases (ELY vs. WLY, red lines). The analysis uses the anomalies, as in Figure 2, defined as deviations from the climatology for all years available. Results show that the composite zonal wind and heat flux anomalies are overall similar between LA and EL, and between ELY and WLY, whereas some differences are statistically significant at the 95% level: UKMO15 has more easterly anomalies around lag = −25 to −15 days for EL compared to LA. This is also the case with WLY compared to ELY. DWD21 exhibits more easterly anomalies around lag = +10 to +25 days for EL than for LA.

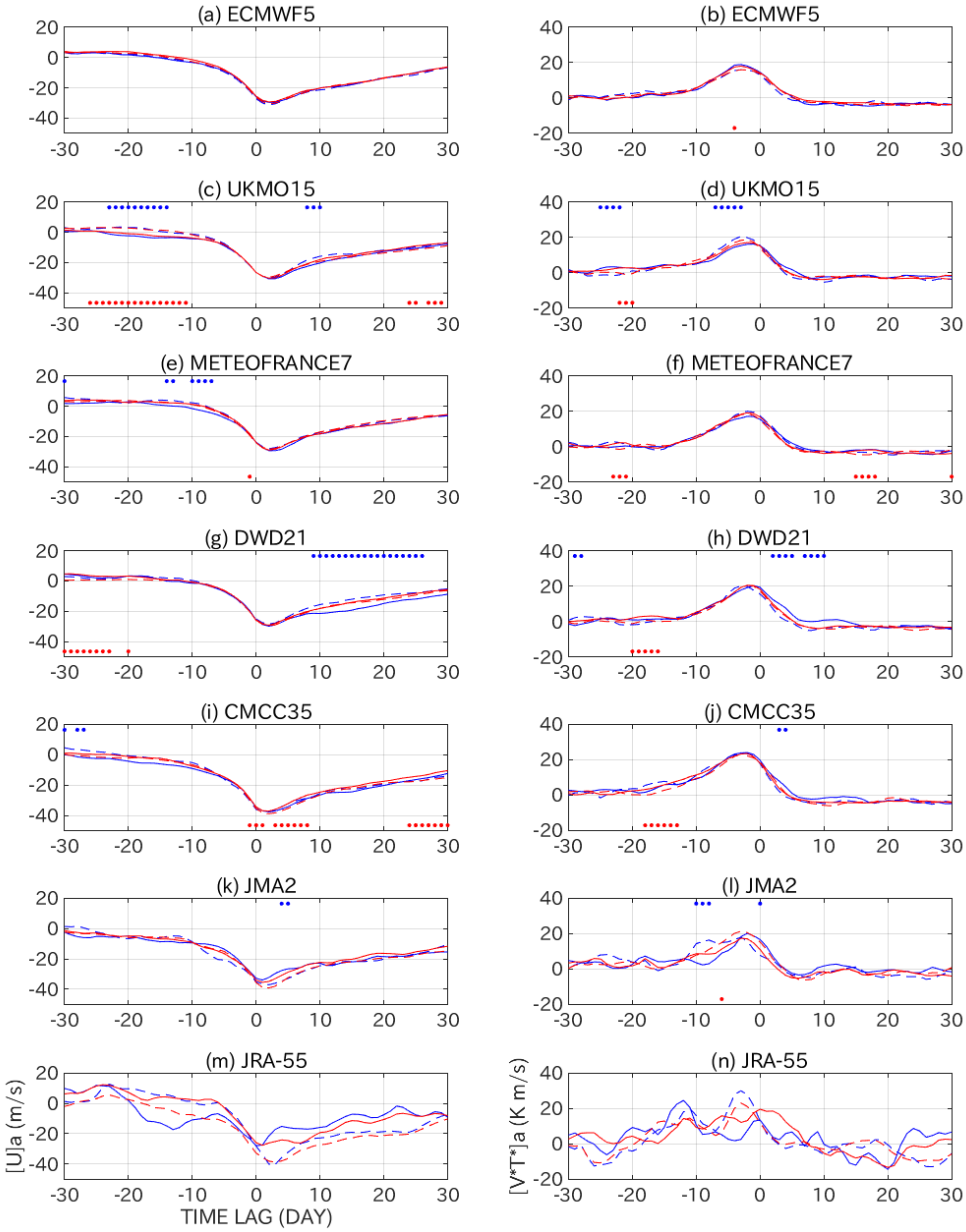


**Figure 8.** (Left panels) Similar to Figure 2d, but using MSSWs separately for LA, EL, ELY, and WLY for each system and JRA-55 data. Blue lines are for LA (broken) and EL (solid), and red lines are for ELY (broken) and WLY (solid). Dots denote significant differences at the 95% level (two side test) between LA and EL (blue dots), or between ELY and WLY (red dots). Right panels are similar, but plot waves 1–3 heat flux anomalies as in Figure 2e.

We compare precursory signals to the MSSWs between LA and EL below, since changes in planetary wave forcing with ENSO were studied in previous studies [53–56]. Figure 9 is similar to Figure 3, but separately uses the LA MSSWs and EL MSSWs. The ellipses are drawn using 25 percentiles of the distance values to emphasize differences between the two conditions. Results for the HC data show that the wave 1 contribution in both mean and precursory signal is larger for EL (dots) than for LA (triangles), whereas the wave 2 counterpart is smaller. This compensation explains the fact that the waves 1–3 heat flux anomalies are overall similar between LA and EL (Figure 8). The enhanced roles of wave 1 for EL and wave 2 for LA were pointed out by previous studies [55,56]. The JRA-55 results are different from the HC results.

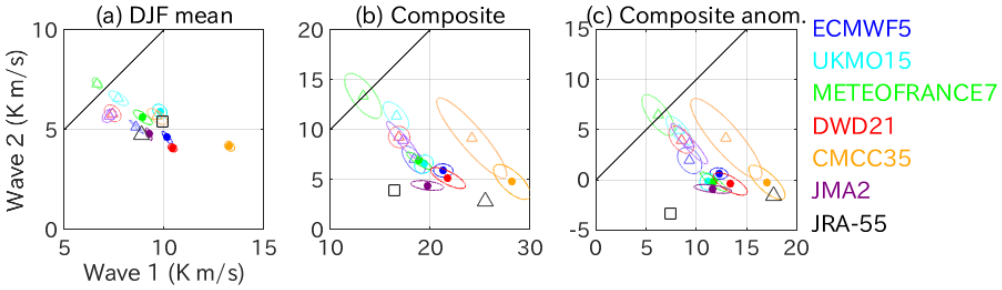


**Figure 9.** Similar to Figure 3, but separately using the LA MSSWs and EL MSSWs: (**a**) DJF climatology, (**b**) MSSW composite heat flux, and (**c**) MSSW composite heat flux anomalies. Thin colors and triangles are used for the MSSWs for LA. Magnitude of each ellipse is based on the 25% distance of the ensemble members.

Figure 10 compares composite GPH anomalies at 500 hPa between the LA MSSWs and EL MSSWs. Results for the HC data commonly exhibit differences of negative values over the north Pacific and positive values over north America. The former, i.e., negative difference over north Pacific reflects more pronounced negative anomalies, i.e., enhanced Aleutian Low for EL. In the JRA-55 result, the negative difference over the north Pacific is located more equatorward, and a positive difference is notable over Alaska. These features reflect pronounced negative anomalies over Alaska for LA and more equatorward location of negative anomalies over the Pacific for EL. An examination of the climatological 500 hPa GPH fields for the LA and EL winters reveals difference patterns like the familiar Pacific North America pattern [57,58], which are similar for all systems and JRA-55 data (not shown). The HC data differences in the composite Z500 anomalies between LA and EL (Figure 10) are similar to those in the climatological states. This similarity is not the case with the JRA-55 data due to the small sample size of the MSSWs.

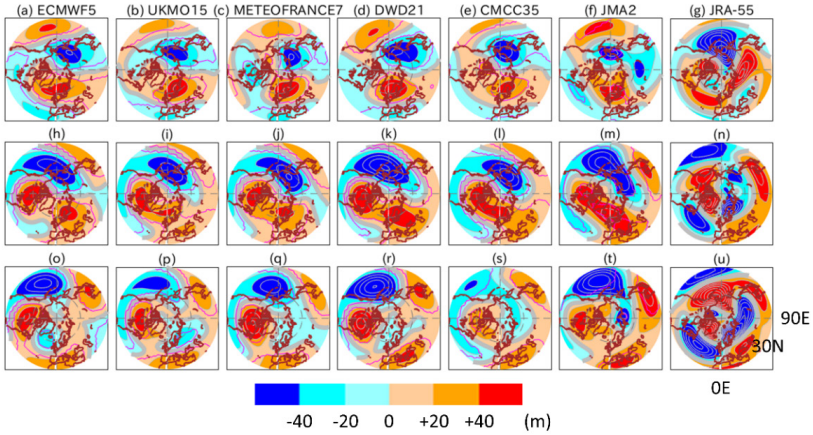


**Figure 10.** Similar to Figure 4, but separately using the LA MSSWs (**a**–**g**) and EL MSSWs (**h**–**n**). Bottom panels (**o**–**u**) plot differences of the EL MSSWs from the LA MSSWs. Magenta contours denote statistically significant anomalies or differences at the 95% level.

Differences in the composite GPH at 10 hPa between the LA MSSWs and EL MSSWs show negative values over the north Atlantic and Europe around 0° E and positive values over northwest America for the five systems, except for ECMWF5 (Figure 11). These patterns indicate that the composite patterns have enhanced wave 1 component for the EL MSSWs, which is consistent with the changes in the troposphere and lower stratosphere (Figures 9 and 10). The positive values over northwest America also imply enhanced wave 2 component for the LA MSSWs. The JRA-55 results exhibit different features from the HC results, e.g., elongated vortex structure for EL (Figure 11m).

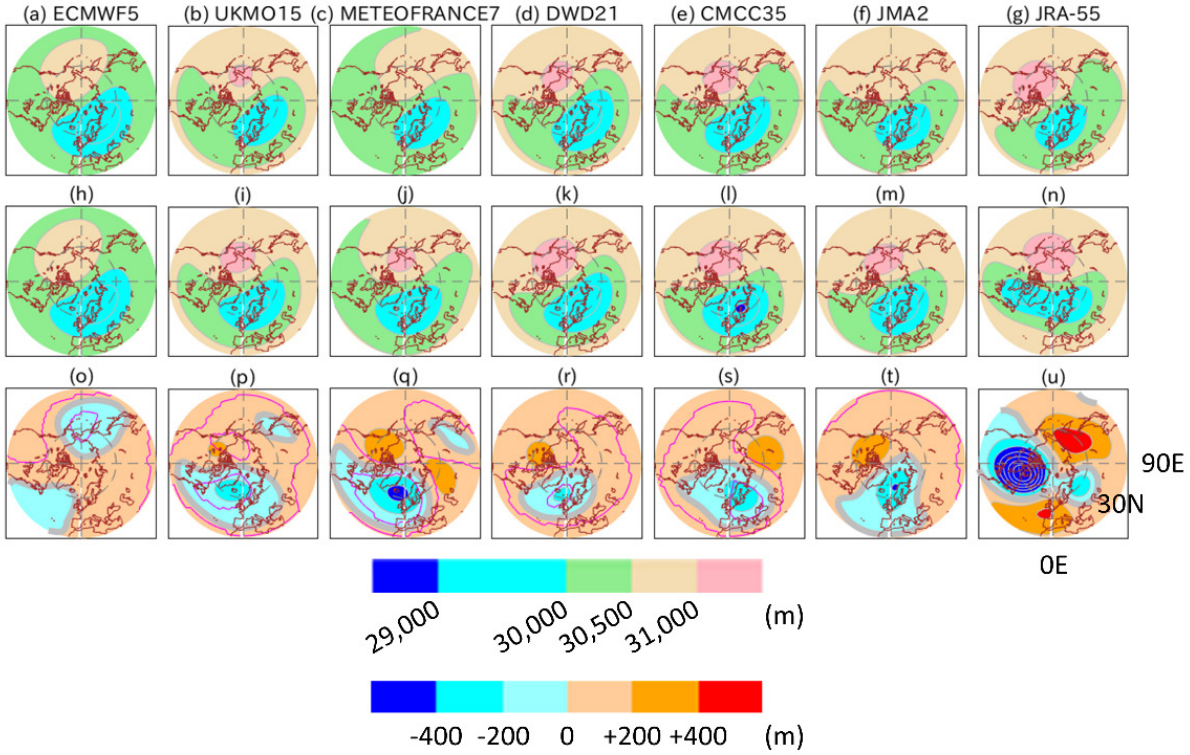


**Figure 11.** Similar to Figure 10, but for the 10 hPa GPH around the MSSW onset date of lag = ±2 days. Panels (**a**–**n**) plot the 10 hPa GPH, and (**o**–**u**) plot its differences. All wave components in addition to the zonal mean are retained.

The teleconnection signals in the mean VS, MSSW frequency, and HFE frequency are examined in detail in Figure 12. The differences are taken between LA and EL, and between ELY and WLY. Regarding the ENSO teleconnection, all six systems show a weaker mean vortex for EL than for LA in the ensemble means. The ensemble mean differences are judged to be significant at high confidence levels, except for JMA2. It is also noted that the 99% range of all systems extends over both positive and negative values, implying that some ensemble members have an opposite result in sign to the ensemble mean result. The mean vortex weakening in the HC data is consistent in both sign and magnitude with the JRA-55 result. Such vortex weakening for El Niño has been observed in [59,60].

The HC data exhibit an increased MSSW frequency for EL than for LA in the ensemble means. The ensemble mean differences are judged to be significant at confidence levels close to, or higher than, 90%, except for JMA2. The JRA-55 data show a decrease in the MSSW frequency, which is opposite to the HC ensemble mean result in sign, but is within or close to the 99% ranges. The JRA-55 result, which is different from [61], is likely to reflect the relatively short target period. The five systems, except for METEOFRANCE7, and JRA-55 data show an increased HFE frequency, although statistical significance of the ensemble mean difference is found only for some of the systems.

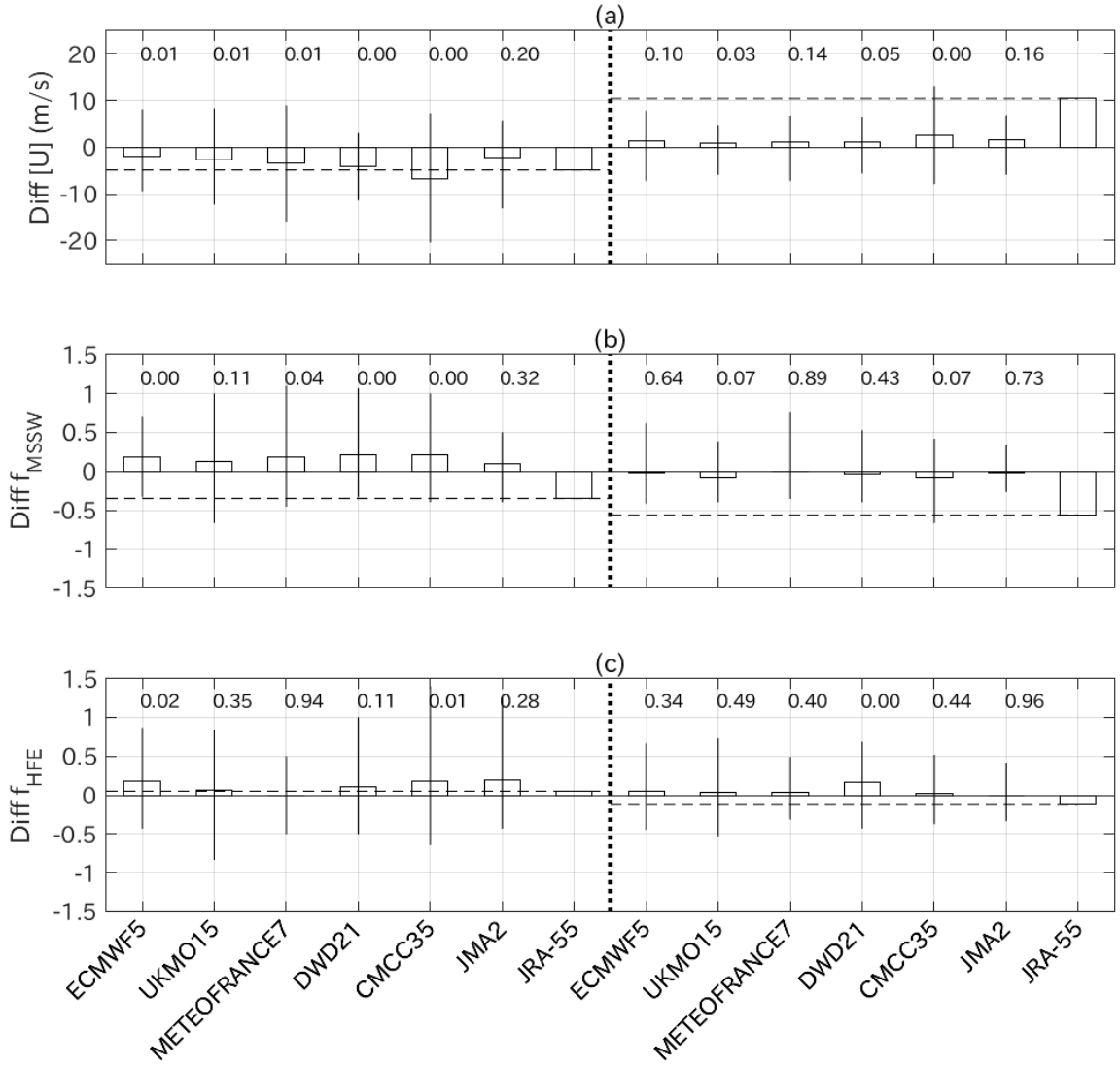


**Figure 12.** Bar charts showing differences of the three quantities as in Figure 7: (**a**) mean VS, (**b**) MSSW frequency, and (**c**) HFE frequency. Seven left bars in each panel plot EL minus LA, and the others plot WLY minus ELY. Number for each bar denotes the *p* value from the *t*-test (two side test) applied to the differences of the ensemble members.

Figure 13a,b examine possible relationships of the MSSW frequency with the mean VS and HFE frequency in the ENSO teleconnection. For example, Figure 13a correlates the EL minus LA differences in the MSSW frequency with those in the mean VS. The differences of these two quantities are negatively correlated when looking at the ensemble members for each system, with values ranging from −0.76 to −0.30 (Table 3). The mean differences of the ensemble have a negative correlation of −0.66. These values suggest that the relationship between the mean VS and MSSW frequency can explain the variability of the ENSO teleconnection, i.e., differences in the MSSW frequency with ENSO, among the ensemble members and also systems. The weakening of the mean VS and the decrease in the MSSW frequency in the JRA-55 data are apparently inconsistent with each other, but such a result emerges in some ensemble members (Figures 12 and 13). This is consistent with [62], who pointed out large differences among ensemble members. An examination of the differences in the MSSW and HFE frequencies shows positive correlations for all systems, although the correlations are judged to be significant only for some systems. The mean differences of the ensemble have a correlation value close to zero among the systems (Figure 13b, Table 3).

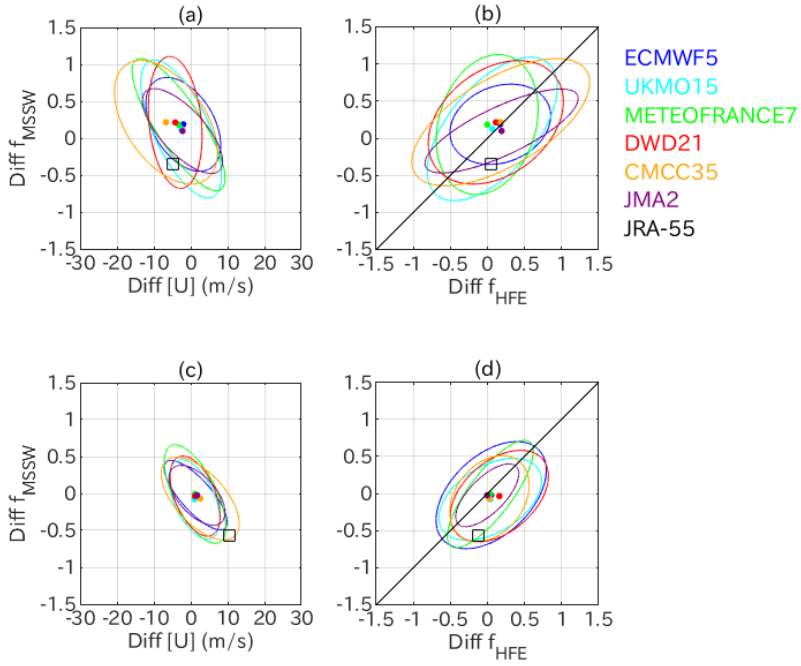


**Figure 13.** (**a**) Similar to Figure 6a, but for EL minus LA differences. Panel (**b**) is similar to (**a**), but use the HFE frequency instead of the mean VS. Panels (**c**,**d**) are similar, but for WLY minus ELY differences.

**Table 3.** Same as Table 2, but for differences between LA and EL, and between ELY and WLY. Asterisk denotes statistical significance at the 95% level.

| System Name | LA and EL Differences | | ELY and WLY Differences | |
|---|---|---|---|---|
| | $f_{MSSW}$ and Mean VS | $f_{MSSW}$ and $f_{HFE}$ | $f_{MSSW}$ and Mean VS | $f_{MSSW}$ and $f_{HFE}$ |
| ECMWF5 | −0.40 * | +0.29 | −0.68 * | +0.44 * |
| UKMO15 | −0.75 * | +0.53 * | −0.42 * | +0.48 * |
| METEOFRANCE7 | −0.76 * | +0.29 | −0.76 * | +0.65 * |
| DWD21 | −0.30 | +0.35 | −0.52 * | +0.46 * |
| CMCC35 | −0.45 * | +0.31 * | −0.63 * | +0.37 * |
| JMA2 | −0.66 * | +0.74 * | −0.49 | +0.59 |
| Ensemble means | −0.66 | −0.053 | −0.29 | +0.057 |

As for the QBO teleconnection, both HC ensemble mean and JRA-55 data exhibit a stronger mean vortex for WLY (Figure 12a). The ensemble mean differences are judged to be significant at a confidence level higher than, or close to, 90% for all systems. The stronger vortex for WLY is consistent with the familiar observational result [40,63]. The JRA-55 result is above the 99% ranges of the five systems and close to the upper end of the range of CMCC35. This means that the JRA-55 result is near the largest differences simulated by the forecast systems. All systems and JRA-55 data show a decreased MSSW frequency for WLY (Figure 12b). Only UKMO15 and CMCC35 have $p$ values smaller than 0.10, i.e., significance at the 90% level. Again, the JRA-55 difference is close to the bottom end of the HC 99% range implying a much stronger response.

The WLY minus ELY differences in the mean VS and MSSW frequency have negative correlations among the ensemble members for all systems (Figure 13c, Table 3). The correlation for the ensemble means is weaker and insignificant. The JRA-55 result is located near the edge of the HC distributions confirming the strongest response of the JRA-55 data.

The HFE frequency shows a significant ensemble mean increase for WLY only for DWD21. This increase is inconsistent with the insignificant change in the MSSW frequency, suggesting that its effect is overwhelmed by another or other factors. The WLY minus ELY differences in the HFE frequency are also positively correlated with those in the MSSW frequency for the ensemble members (Figure 13d, Table 3), but not for the ensemble means.

## 4. Discussion

This study has investigated intra-seasonal variations of MSSWs in the HC and JRA-55 data, and demonstrated that all systems more or less reproduce precursory signals that are similar to the JRA-55 results. This is consistent with the good reproducibility of the coupling of the stratospheric polar vortex variability with the lower stratospheric wave activity variability in the HC data shown by [30]. The reproducibility of the present systems seems better than the North American Multi-Model Ensemble Phase-2 models examined by [29]. This will be explained at least partly by the fact that the present systems have higher resolution in horizontal resolution, top level, and number of vertical levels. This speculation is consistent with [26], who pointed out better reproducibility of stratospheric variability by high-top models. Relative importance of these factors remains to be further studied.

It is interesting to note that three MSSWs occur in a couple of DJF seasons (years) in the HC data (not shown), which has not been observed in [15]. This may be just a lack of sample size in observational and reanalysis data, but may be a manifestation of model biases. In the latter case, the systems may allow MSSWs or notable heat flux events to occur too repeatedly.

Analysis has shown that the ensemble mean MSSW frequency in the HC data is distributed around the JRA-55 counterpart, and varies among the systems. The MSSW frequency also varies among the ensemble members for each system. This study has not only confirmed the importance of the mean VS in explaining such variations in the MSSW frequency as in [24,31–33] but also pointed out that of the HFE frequency. The HFE frequency is a manifestation of transient variability and can be interpreted as another factor for MSSW frequency [33]. It will be interesting to try to construct a statistical model to reproduce, or predict, MSSW frequency using these factors, and this task is left for future work.

The ENSO teleconnection signals found for the HC data in this study show a weakening of the mean VS and an increase in the MSSW frequency in the ensemble means with increase in the NINO3.4 index. Respective ensemble members have both signs of changes in the mean VS and MSSW frequency between LA and EL. The JRA-55 results, i.e., weakening of the mean VS and decrease in the MSSW frequency, are included in, or located near, the ensemble spread: some ensemble members exhibit such apparently inconsistent results. This suggests a difficulty in identifying teleconnection signals, especially for MSSW frequency, in limited observational records of just one realization as pointed out by [62]. The situation is similar for the QBO teleconnections signals. Both HC ensemble mean and JRA-55 data show an increase in the mean VS and a decrease in the MSSW frequency for WLY rather than for ELY. The JRA-55 results are larger in magnitude than the results from most ensemble members, consistent with [22,30].

One could extend the present analysis of the teleconnections by considering seasonality, and sensitivity to the indices and thresholds. One could also take account of other factors in addition to ENSO and QBO, such as the Madden Julian Oscillation [64,65] and snow/sea ice conditions [66,67]. These are beyond the scope of this study, and are left to future work. Furthermore, this study leaves a question as to if, and how, the QBO affects the intra-seasonal variations of the MSSWs.

This study has examined climatological and teleconnection aspects of the seasonal HC data, but not forecast properties, such as forecast skill. Previous studies of sub-seasonal forecasts showed that a typical predictable time period for MSSWs is one week to 10 days [68,69]. The time period is here referred to as the timing for which half of ensemble members successfully forecast target MSSWs. Seasonal forecasts for MSSW occurrence or absence were

examined in [30,70]. Since the present forecast systems turn out to have biases, e.g., in the mean VS and teleconnection signals, an interesting issue will be if and how such biases are related to forecast properties. For example, Taguchi [70] found that skill of a seasonal forecast system for extratropical stratospheric variability changed with the observed phase of the QBO, and suggested that the change might reflect the reality of the QBO teleconnection in the forecast data. This issue is under investigation, and will be reported in a separate paper. Furthermore, results from recent studies implied that unresolved, parametrized eddy mixing may be a candidate affecting the polar vortex variability and MSSW occurrence, and hence forecast skill for them [71,72].

## 5. Conclusions

This study has investigated intra-seasonal variations and occurrence frequency of MSSWs in Northern winter seasonal HC data of six systems from 1993/1994 to 2016/2017. The investigation has been conducted from both climatological and teleconnection perspectives, in comparison to the JRA-55 data. The teleconnection perspective deals with ENSO and QBO as external factors.

Results for climatological features show that all six systems overall reproduce precursory signals to the MSSWs well, such as increase in the planetary wave heat flux in the extratropical lower stratosphere and anomalous planetary wave patterns in the tropospheric circulation. An underestimation or overestimation of the mean MSSW frequency is suggested, depending on the systems. Such differences in the MSSW frequency among the systems are related to those in the mean VS, and may also be partly contributed by those in the HFE frequency. The MSSW frequency is related to the mean VS and HFE frequency among the ensemble members for most systems.

Regarding teleconnection, the composite times series of the VS and heat flux are found to be overall similar between LA and EL, and between ELY and WLY. Relative contributions from wave 1 and wave 2 to the enhanced heat flux to the MSSWs change with ENSO: wave 1 contribution becomes more important for EL, and the contribution from wave 2 increases for LA. These changes are consistent with the climatological response of the extratropical troposphere to ENSO resembling the Pacific North America pattern.

Analysis of the HC ensemble means shows a weaker mean vortex and an increased MSSW frequency for EL than for LA. The mean vortex weakening for EL is consistent with the JRA-55 data, in which the MSSW frequency decreases in the 24-year period. Such JRA-55 results are included near the edge of the distributions of the ensemble members. The mean results of the ensemble qualitatively reproduce the familiar QBO teleconnection, i.e., weaker VS and increased MSSW frequency for ELY than that for WLY. The JRA-55 results are near the strongest responses of the ensemble members. The changes in the MSSW frequency with ENSO and QBO are correlated to those in the mean VS among the ensemble members and also the ensemble means for some systems. Changes in the HFE frequency are also suggested to play a role in the ensemble spread of the MSSW frequency.

**Funding:** This study was partly supported by JSPS Grant-in-Aid for Scientific Research (C) 22K03719.

**Data Availability Statement:** The data used for this study are available as follows. The JRA-55 data were obtained from the Research Data Archive at the National Center for Atmospheric Research, Computational and Information Systems Laboratory at https://doi.org/10.5065/D6HH6H41, accessed on 31 March 2022. The NINO3.4 data were obtained from the NOAA/CPC monthly atmospheric and SST indices at https://www.cpc.ncep.noaa.gov/data/indices/ersst5.nino.mth.91-20.ascii, accessed on 31 March 2022. The HC data were obtained from the C3S database at https://cds.climate.copernicus.eu/cdsapp#!/home, accessed on 31 March 2022.

**Acknowledgments:** The author thanks those who made the data for this study available: Japan Meteorological Agency for the JRA-55 data, NOAA/CPC for the NINO3.4 data, and C3S service for the HC data.

**Conflicts of Interest:** The author declares no conflict of interest.

## References


1. Baldwin, M.P.; Ayarzagüena, B.; Birner, T.; Butchart, N.; Butler, A.H.; Charlton-Perez, A.J.; Domeisen, D.I.V.; Garfinkel, C.I.; Garny, H.; Gerber, E.P.; et al. Sudden Stratospheric Warmings. *Rev. Geophys.* **2021**, *59*, e2020RG000708. [CrossRef]
2. Matsuno, T. Vertical Propagation of Stationary Planetary Waves in the Winter Northern Hemisphere. *J. Atmos. Sci.* **1970**, *27*, 871–883. [CrossRef]
3. Matsuno, T. A Dynamical Model of the Stratospheric Sudden Warming. *J. Atmos. Sci.* **1971**, *28*, 1479–1494. [CrossRef]
4. Andrews, D.G.; Holton, J.R.; Leovy, C.B. *Middle Atmosphere Dynamics*; Academic Press: Cambridge, MA, USA, 1987.
5. Baldwin, M.P.; Dunkerton, T.J. Stratospheric Harbingers of Anomalous Weather Regimes. *Science* **2001**, *294*, 581–584. [CrossRef]
6. Polvani, L.M.; Waugh, D.W. Upward Wave Activity Flux as a Precursor to Extreme Stratospheric Events and Subsequent Anomalous Surface Weather Regimes. *J. Clim.* **2004**, *17*, 3548–3554. [CrossRef]
7. Kidston, J.; Scaife, A.A.; Hardiman, S.C.; Mitchell, D.M.; Butchart, N.; Baldwin, M.P.; Gray, L.J. Stratospheric Influence on Tropospheric Jet Streams, Storm Tracks and Surface Weather. *Nat. Geosci.* **2015**, *8*, 433–440. [CrossRef]
8. Song, Y.; Robinson, W.A. Dynamical Mechanisms for Stratospheric Influences on the Troposphere. *J. Atmos. Sci.* **2004**, *61*, 1711–1725. [CrossRef]
9. Hitchcock, P.; Simpson, I.R. The Downward Influence of Stratospheric Sudden Warmings. *J. Atmos. Sci.* **2014**, *71*, 3856–3876. [CrossRef]
10. Ogawa, F.; Omrani, N.E.; Nishii, K.; Nakamura, H.; Keenlyside, N. Ozone-Induced Climate Change Propped up by the Southern Hemisphere Oceanic Front. *Geophys. Res. Lett.* **2015**, *42*, 10056–10063. [CrossRef]
11. Kunz, T.; Greatbatch, R.J. On the Northern Annular Mode Surface Signal Associated with Stratospheric Variability. *J. Atmos. Sci.* **2013**, *70*, 2103–2118. [CrossRef]
12. Wittman, M.A.H.; Polvani, L.M.; Scott, R.K.; Charlton, A.J. Stratospheric Influence on Baroclinic Lifecylces and Its Connection to the Arctic Oscillation. *Geophys. Res. Lett.* **2004**, *31*, L16113. [CrossRef]
13. Lubis, S.W.; Huang, C.S.Y.; Nakamura, N.; Jucker, M. Role of Finite-Amplitude Rossby Waves and Nonconservative Processes in Downward Migration of Extratropical Flow Anomalies. *J. Atmos. Sci.* **2018**, *75*, 1385–1401. [CrossRef]
14. Charlton, A.J.; Polvani, L.M. A New Look at Stratospheric Sudden Warmings. Part I: Climatology and Modeling Benchmarks. *J. Clim.* **2007**, *20*, 449–469. [CrossRef]
15. Butler, A.H.; Sjoberg, J.P.; Seidel, D.J.; Rosenlof, K.H. A Sudden Stratospheric Warming Compendium. *Earth Syst. Sci. Data* **2017**, *9*, 63–76. [CrossRef]
16. Sigmond, M.; Scinocca, J.; Kharin, V.; Shepherd, T. Enhanced Seasonal Forecast Skill Following Stratospheric Sudden Warmings. *Nat. Geosci.* **2013**, *6*, 98–102. [CrossRef]
17. Tripathi, O.P.; Charlton-Perez, A.; Sigmond, M.; Vitart, F. Enhanced Long-Range Forecast Skill in Boreal Winter Following Stratospheric Strong Vortex Conditions. *Environ. Res. Lett.* **2015**, *10*, 104007. [CrossRef]
18. Domeisen, D.I.V.; Butler, A.H.; Fröhlich, K.; Bittner, M.; Müller, W.A.; Baehr, J. Seasonal Predictability over Europe Arising from El Niño and Stratospheric Variability in the MPI-ESM Seasonal Prediction System. *J. Clim.* **2015**, *28*, 256–271. [CrossRef]
19. Scaife, A.A.; Karpechko, A.Y.; Baldwin, M.P.; Brookshaw, A.; Butler, A.H.; Eade, R.; Gordon, M.; Maclachlan, C.; Martin, N.; Dunstone, N.; et al. Seasonal Winter Forecasts and the Stratosphere. *Atmos. Sci. Lett.* **2016**, *17*, 51–56. [CrossRef]
20. Mukougawa, H.; Hirooka, T.; Kuroda, Y. Influence of Stratospheric Circulation on the Predictability of the Tropospheric Northern Annular Mode. *Geophys. Res. Lett.* **2009**, *36*, L08814. [CrossRef]
21. Rao, J.; Garfinkel, C.I. CMIP5/6 Models Project Little Change in the Statistical Characteristics of Sudden Stratospheric Warmings in the 21st Century. *Environ. Res. Lett.* **2021**, *16*, 034024. [CrossRef]
22. Anstey, J.A.; Simpson, I.R.; Richter, J.H.; Naoe, H.; Taguchi, M.; Serva, F.; Gray, L.J.; Butchart, N.; Hamilton, K.; Osprey, S.; et al. Teleconnections of the Quasi-Biennial Oscillation in a Multi-Model Ensemble of QBO-Resolving Models. *Q. J. R. Meteorol. Soc.* **2021**, *148*, 1568–1592. [CrossRef]
23. Domeisen, D.I.V.; Butler, A.H.; Charlton-Perez, A.J.; Ayarzagüena, B.; Baldwin, M.P.; Dunn-Sigouin, E.; Furtado, J.C.; Garfinkel, C.I.; Hitchcock, P.; Karpechko, A.Y.; et al. The Role of the Stratosphere in Subseasonal to Seasonal Prediction: 1. Predictability of the Stratosphere. *J. Geophys. Res. Atmos.* **2020**, *125*, e2019JD030920. [CrossRef]
24. Wu, Z.; Reichler, T. Variations in the Frequency of Stratospheric Sudden Warmings in CMIP5 and CMIP6 and Possible Causes. *J. Clim.* **2020**, *33*, 10305–10320. [CrossRef]
25. Ayarzagüena, B.; Charlton-Perez, A.J.; Butler, A.H.; Hitchcock, P.; Simpson, I.R.; Polvani, L.M.; Butchart, N.; Gerber, E.P.; Gray, L.; Hassler, B.; et al. Uncertainty in the Response of Sudden Stratospheric Warmings and Stratosphere-Troposphere Coupling to Quadrupled $CO_2$ Concentrations in CMIP6 Models. *J. Geophys. Res. Atmos.* **2020**, *125*, e2019JD032345. [CrossRef]
26. Charlton-Perez, A.J.; Baldwin, M.P.; Birner, T.; Black, R.X.; Butler, A.H.; Calvo, N.; Davis, N.A.; Gerber, E.P.; Gillett, N.; Hardiman, S.; et al. On the Lack of Stratospheric Dynamical Variability in Low-Top Versions of the CMIP5 Models. *J. Geophys. Res. Atmos.* **2013**, *118*, 2494–2505. [CrossRef]
27. Seviour, W.J.M.; Gray, L.J.; Mitchell, D.M. Stratospheric Polar Vortex Splits and Displacements in the High-Top CMIP5 Climate Models. *J. Geophys. Res. Atmos.* **2016**, *121*, 1400–1413. [CrossRef]
28. Maycock, A.C.; Keeley, S.P.E.; Charlton-Perez, A.J.; Doblas-Reyes, F.J. Stratospheric Circulation in Seasonal Forecasting Models: Implications for Seasonal Prediction. *Clim. Dyn.* **2011**, *36*, 309–321. [CrossRef]

29. Furtado, J.C.; Cohen, J.; Becker, E.J.; Collins, D.C. Evaluating the Relationship between Sudden Stratospheric Warmings and Tropospheric Weather Regimes in the NMME Phase-2 Models. *Clim. Dyn.* **2021**, *56*, 2321–2338. [CrossRef]
30. Portal, A.; Ruggieri, P.; Palmeiro, F.M.; García-Serrano, J.; Domeisen, D.I.V.; Gualdi, S. Seasonal Prediction of the Boreal Winter Stratosphere. *Clim. Dyn.* **2021**, *58*, 2109–2130. [CrossRef]
31. Mclandress, C.; Shepherd, T.G. Impact of Climate Change on Stratospheric Sudden Warmings as Simulated by the Canadian Middle Atmosphere Model. *J. Clim.* **2009**, *22*, 5449–5463. [CrossRef]
32. Kim, J.; Son, S.W.; Gerber, E.P.; Park, H.S. Defining Sudden Stratospheric Warming in Climate Models: Accounting for Biases in Model Climatologies. *J. Clim.* **2017**, *30*, 5529–5546. [CrossRef]
33. Taguchi, M. A Study of Different Frequencies of Major Stratospheric Sudden Warmings in CMIP5 Historical Simulations. *J. Geophys. Res.* **2017**, *122*, 5144–5156. [CrossRef]
34. Domeisen, D.I.V.; Garfinkel, C.I.; Butler, A.H. The Teleconnection of El Niño Southern Oscillation to the Stratosphere. *Rev. Geophys.* **2019**, *57*, 5–47. [CrossRef]
35. Butler, A.H.; Arribas, A.; Athanassiadou, M.; Baehr, J.; Calvo, N.; Charlton-Perez, A.; Déqué, M.; Domeisen, D.I.V.; Fröhlich, K.; Hendon, H.; et al. The Climate-System Historical Forecast Project: Do Stratosphere-Resolving Models Make Better Seasonal Climate Predictions in Boreal Winter? *Q. J. R. Meteorol. Soc.* **2016**, *142*, 1413–1427. [CrossRef]
36. Anstey, J.A.; Shepherd, T.G. High-Latitude Influence of the Quasi-Biennial Oscillation. *Q. J. R. Meteorol. Soc.* **2014**, *140*, 1–21. [CrossRef]
37. Naoe, H.; Shibata, K. Equatorial Quasi-Biennial Oscillation Influence on Northern Winter Extratropical Circulation. *J. Geophys. Res. Atmos.* **2010**, *115*. [CrossRef]
38. Garfinkel, C.I.; Shaw, T.A.; Hartmann, D.L.; Waugh, D.W. Does the Holton-Tan Mechanism Explain How the Quasi-Biennial Oscillation Modulates the Arctic Polar Vortex? *J. Atmos. Sci.* **2012**, *69*, 1713–1733. [CrossRef]
39. Watson, P.A.G.; Gray, L.J. How Does the Quasi-Biennial Oscillation Affect the Stratospheric Polar Vortex? *J. Atmos. Sci.* **2014**, *71*, 391–409. [CrossRef]
40. Holton, J.R.; Tan, H.-C. The Influence of the Equatorial Quasi-Biennial Oscillation on the Global Circulation at 50 Mb. *J. Atmos. Sci.* **1980**, *37*, 2200–2208. [CrossRef]
41. Silverman, V.; Harnik, N.; Matthes, K.; Lubis, S.W.; Wahl, S. Radiative Effects of Ozone Waves on the Northern Hemisphere Polar Vortex and Its Modulation by the QBO. *Atmos. Chem. Phys.* **2018**, *18*, 6637–6659. [CrossRef]
42. Fereday, D.R.; Maidens, A.; Arribas, A.; Scaife, A.A.; Knight, J.R. Seasonal Forecasts of Northern Hemisphere Winter 2009/10. *Environ. Res. Lett.* **2012**, *7*, 034031. [CrossRef]
43. Rao, J.; Garfinkel, C.I.; Wu, T.; Lu, Y.; Lu, Q.; Liang, Z. The January 2021 Sudden Stratospheric Warming and Its Prediction in Subseasonal to Seasonal Models. *J. Geophys. Res. Atmos.* **2021**, *126*, e2021JD035057. [CrossRef]
44. Kobayashi, S.; Ota, Y.; Harada, Y.; Ebita, A.; Moriya, M.; Onoda, H.; Onogi, K.; Kamahori, H.; Kobayashi, C.; Endo, H.; et al. The JRA-55 Reanalysis: General Specifications and Basic Characteristics. *J. Meteorol. Soc. Japan. Ser. II* **2015**, *93*, 5–48. [CrossRef]
45. Ayarzagüena, B.; Palmeiro, F.M.; Barriopedro, D.; Calvo, N.; Langematz, U.; Shibata, K. On the Representation of Major Stratospheric Warmings in Reanalyses. *Atmos. Chem. Phys.* **2019**, *19*, 9469–9484. [CrossRef]
46. Butler, A.H.; Seidel, D.J.; Hardiman, S.C.; Butchart, N.; Birner, T.; Match, A. Defining Sudden Stratospheric Warmings. *Bull. Am. Meteorol. Soc.* **2015**, *96*, 1913–1928. [CrossRef]
47. Shen, X.; Wang, L.; Osprey, S. Tropospheric Forcing of the 2019 Antarctic Sudden Stratospheric Warming. *Geophys. Res. Lett.* **2020**, *47*, e2020GL089343. [CrossRef]
48. Nishii, K.; Nakamura, H. Tropospheric Influence on the Diminished Antarctic Ozone Hole in September 2002. *Geophys. Res. Lett.* **2004**, *31*, L16103. [CrossRef]
49. Nishii, K.; Nakamura, H.; Miyasaka, T. Modulations in the Planetary Wave Field Induced by Upward-Propagating Rossby Wave Packets Prior to Stratospheric Sudden Warming Events: A Case-Study. *Q. J. R. Meteorol. Soc.* **2009**, *135*, 39–52. [CrossRef]
50. Smith, K.L.; Kushner, P.J.; Cohen, J. The Role of Linear Interference in Northern Annular Mode Variability Associated with Eurasian Snow Cover Extent. *J. Clim.* **2011**, *24*, 6185–6202. [CrossRef]
51. Kolstad, E.W.; Charlton-Perez, A.J. Observed and Simulated Precursors of Stratospheric Polar Vortex Anomalies in the Northern Hemisphere. *Clim. Dyn.* **2011**, *37*, 1443–1456. [CrossRef]
52. Cohen, J.; Jones, J. Tropospheric Precursors and Stratospheric Warmings. *J. Clim.* **2011**, *24*, 6562–6572. [CrossRef]
53. Sassi, F.; Kinnison, D.; Boville, B.A.; Garcia, R.R.; Roble, R. Effect of El Niño-Southern Oscillation on the Dynamical, Thermal, and Chemical Structure of the Middle Atmosphere. *J. Geophys. Res. D Atmos.* **2004**, *109*, D17108. [CrossRef]
54. Manzini, E.; Giorgetta, M.A.; Esch, M.; Kornblueh, L.; Roeckner, E. The Influence of Sea Surface Temperatures on the Northern Winter Stratosphere: Ensemble Simulations with the MAECHAM5 Model. *J. Clim.* **2006**, *19*, 3863–3881. [CrossRef]
55. Taguchi, M.; Hartmann, D.L. Increased Occurrence of Stratospheric Sudden Warmings during El Niño as Simulated by WACCM. *J. Clim.* **2006**, *19*, 324–332. [CrossRef]
56. Barriopedro, D.; Calvo, N. On the Relationship between ENSO, Stratospheric Sudden Warmings, and Blocking. *J. Clim.* **2014**, *27*, 4704–4720. [CrossRef]
57. Barnston, A.G.; Livezey, R.E. Classification, Seasonality and Persistence of Low-Frequency Atmospheric Circulation Patterns. *Mon. Weather Rev.* **1987**, *115*, 1083–1126. [CrossRef]

58. Horel, J.D.; Wallace, J.M. Planetary-Scale Atmospheric Phenomena Associated with the Southern Oscillation. *Mon. Weather Rev.* **1981**, *109*, 813–829. [CrossRef]
59. Camp, C.D.; Tung, K.K. Stratospheric Polar Warming by ENSO in Winter: A Statistical Study. *Geophys. Res. Lett.* **2007**, *34*, L04809. [CrossRef]
60. Garfinkel, C.I.; Hartmann, D.L. Effects of the El Niño-Southern Oscillation and the Quasi-Biennial Oscillation on Polar Temperatures in the Stratosphere. *J. Geophys. Res. Atmos.* **2007**, *112*, D19112. [CrossRef]
61. Butler, A.H.; Polvani, L.M. El Niño, La Niña, and Stratospheric Sudden Warmings: A Reevaluation in Light of the Observational Record. *Geophys. Res. Lett.* **2011**, *38*, L13807. [CrossRef]
62. Polvani, L.M.; Sun, L.; Butler, A.H.; Richter, J.H.; Deser, C. Distinguishing Stratospheric Sudden Warmings from ENSO as Key Drivers of Wintertime Climate Variability over the North Atlantic and Eurasia. *J. Clim.* **2017**, *30*, 1959–1969. [CrossRef]
63. Holton, J.R.; Tan, H.-C. The Quasi-Biennial Oscillation in the Northern Hemisphere Lower Stratosphere. *J. Meteorol. Soc. Japan. Ser. II* **1982**, *60*, 140–148. [CrossRef]
64. Garfinkel, C.I.; Schwartz, C. MJO-Related Tropical Convection Anomalies Lead to More Accurate Stratospheric Vortex Variability in Subseasonal Forecast Models. *Geophys. Res. Lett.* **2017**, *44*, 10054–10062. [CrossRef]
65. Garfinkel, C.I.; Feldstein, S.B.; Waugh, D.W.; Yoo, C.; Lee, S. Observed Connection between Stratospheric Sudden Warmings and the Madden-Julian Oscillation. *Geophys. Res. Lett.* **2012**, *39*, L18807. [CrossRef]
66. Cohen, J.; Furtado, J.C.; Jones, J.; Barlow, M.; Whittleston, D.; Entekhabi, D. Linking Siberian Snow Cover to Precursors of Stratospheric Variability. *J. Clim.* **2014**, *27*, 5422–5432. [CrossRef]
67. Kim, B.M.; Son, S.W.; Min, S.K.; Jeong, J.H.; Kim, S.J.; Zhang, X.; Shim, T.; Yoon, J.H. Weakening of the Stratospheric Polar Vortex by Arctic Sea-Ice Loss. *Nat. Commun.* **2014**, *5*, 4646. [CrossRef]
68. Karpechko, A.Y. Predictability of Sudden Stratospheric Warmings in the ECMWF Extended-Range Forecast System. *Mon. Weather Rev.* **2018**, *146*, 1063–1075. [CrossRef]
69. Taguchi, M. Predictability of Major Stratospheric Sudden Warmings: Analysis Results from JMA Operational 1-Month Ensemble Predictions from 2001/02 to 2012/13. *J. Atmos. Sci.* **2016**, *73*, 789–806. [CrossRef]
70. Taguchi, M. Seasonal Winter Forecasts of the Northern Stratosphere and Troposphere: Results from JMA Seasonal Hindcast Experiments. *J. Atmos. Sci.* **2018**, *75*, 827–840. [CrossRef]
71. Lubis, S.W.; Huang, C.S.Y.; Nakamura, N. Role of Finite-Amplitude Eddies and Mixing in the Life Cycle of Stratospheric Sudden Warmings. *J. Atmos. Sci.* **2018**, *75*, 3987–4003. [CrossRef]
72. Nakamura, N.; Falk, J.; Lubis, S.W. Why Are Stratospheric Sudden Warmings Sudden (and Intermittent)? *J. Atmos. Sci.* **2020**, *77*, 943–964. [CrossRef]